

## Emergence of explosive synchronization bombs in networks of oscillators

Lluís Arola-Fernández<sup>1,6</sup>, Sergio Faci-Lázaro<sup>2,3</sup>, Per Sebastian Skardal <sup>4</sup>, Emanuel-Cristian Boghiu<sup>5</sup>,  
Jesús Gómez-Gardeñes <sup>2,3</sup>✉ & Alex Arenas <sup>1</sup>✉

Research on network percolation and synchronization has deepened our understanding of abrupt changes in the macroscopic properties of complex engineered and natural systems. While explosive percolation emerges from localized structural perturbations that delay the formation of a connected component, explosive synchronization is usually studied by fine-tuning of global parameters. Here, we introduce the concept of synchronization bombs as large networks of heterogeneous oscillators that abruptly transit from incoherence to phase-locking (or vice-versa) by adding (or removing) one or a few links. We build these bombs by optimizing global synchrony with decentralized information in a competitive percolation process driven by a local rule, and show their occurrence in systems of Kuramoto –periodic– and Rössler –chaotic– oscillators and in a model of cardiac pacemaker cells, providing an analytical characterization in the Kuramoto case. Our results propose a self-organized approach to design and control abrupt transitions in adaptive biological systems and electronic circuits, and place explosive synchronization and percolation under the same mechanistic framework.

<sup>1</sup>Departament d'Enginyeria Informàtica i Matemàtiques, Universitat Rovira i Virgili, 43007 Tarragona, Spain. <sup>2</sup>Department of Condensed Matter Physics, University of Zaragoza, 50009 Zaragoza, Spain. <sup>3</sup>GOTHAM Lab, Institute of Biocomputation and Physics of Complex Systems, University of Zaragoza, 50018 Zaragoza, Spain. <sup>4</sup>Department of Mathematics, Trinity College, Hartford, CT 06106, USA. <sup>5</sup>ICFO—Institut de Ciències Fotòniques, The Barcelona Institute of Science and Technology, 08860 Castelldefels, Barcelona, Spain. <sup>6</sup>Present address: Instituto de Física Interdisciplinar y Sistemas Complejos IFISC (CSIC-UIB), Campus UIB, 07122 Palma de Mallorca, Spain. ✉email: [gardenes@unizar.es](mailto:gardenes@unizar.es); [alexandre.arenas@urv.cat](mailto:alexandre.arenas@urv.cat)

The emergence of abrupt, explosive transitions in the macroscopic behavior of complex networked systems is a fascinating phenomenon, ubiquitous in fields ranging from neuroscience to biology and engineering. There is increasing empirical evidence that explosive synchronization in brain activity is associated with the onset of anesthetic-induced unconsciousness<sup>1–3</sup>, epileptic seizures<sup>4,5</sup> and fibromyalgia<sup>6</sup> and it explains biological switches displaying abrupt responses to external perturbations<sup>7</sup>. Also, in infrastructural and power-grids networks, it is crucial to detect and control small vulnerabilities that can lead to abrupt structural damages and global desynchronization blackouts<sup>8,9</sup>.

From a theoretical perspective, explosive percolation—an abrupt growth of the giant component of the network induced by the addition or removal of single links—was found to occur when competitive rules are applied on the choice of the links in a way that the formation of a giant cluster is delayed<sup>10</sup>. The discovery of this abrupt structural transition, which was shown to be continuous in the thermodynamic limit but with anomalous scaling properties, triggered further analyses to understand the mechanisms that can lead to the explosive behavior in the network growth. In parallel, abrupt transitions were explored in the collective dynamics of the system when considering a physical process among the units, as the spreading of a disease<sup>11–13</sup>, opinion diffusion<sup>14</sup> or traffic flow<sup>15,16</sup>, to name a few<sup>17,18</sup>.

A particularly suitable framework to model the birth of explosive transitions is the synchronization process of coupled oscillators. The phenomena of collective synchronization are widely spread in natural, social and technological systems<sup>19,20</sup>. Its ubiquity has attracted the interest of the physics community, that have tackled its study through minimal models that capture the transition between a disordered phase and coherent dynamics. For populations of heterogeneous phase-oscillators coupled all-to-all<sup>19,20</sup>, abrupt transitions in synchrony as the coupling parameter is increased were found to occur for a uniform distribution of frequencies<sup>21</sup> and the hysteresis cycle involving incoherence and partial synchrony was exactly characterized for a bimodal distribution with a shallow dip<sup>22</sup>. However, the bistable nature of explosive synchronization—an abrupt jump from incoherence to global synchrony induced by a change in the coupling parameter among the units, with an associated hysteresis cycle—was firstly discovered for scale-free networks (i.e. networks with very heterogeneous degree distributions) in the presence of positive correlations between the internal frequencies and the nodal degrees<sup>23</sup>. Further analyses showed that this is only one of the possible mechanisms that inhibit the emergence of a large synchronization cluster, and it was found that, by imposing frequency anti-correlations among connected units in the form of frequency gaps<sup>24</sup> or adaptive anti-Hebbian rules for the weights<sup>25</sup>, explosive transitions occur as the coupling constant is tuned. Furthermore, explosive transitions can also appear in multilayer and dynamically coupled systems<sup>26,27</sup> and they can be enhanced by the presence of noise<sup>28</sup> and higher-order -beyond pair-wise- interactions<sup>29</sup>.

While our fundamental understanding of explosive synchronization has significantly increased in the last years, some key questions remain open. Due to the analytical challenges of studying synchronization dynamics on arbitrary complex networks, a rigorous framework analogous to explosive percolation is still missing<sup>17</sup>. Research on explosive synchronization and percolation has focused on different aspects of the system, namely in the abrupt changes on the macroscopic dynamical or structural properties, respectively, when subject to small variations of the control parameter (the coupling strength or the density of links). Interestingly, in ref. <sup>30</sup>, the authors found that a particular choice of frequency-dependent coupling (which again induces anti-correlations) produces an explosive synchronization process where

the formation of synchronized clusters is delayed analogously to its percolation counterpart. While these results unveiled a connection between both phenomena, the specific model used in ref. <sup>30</sup> is tailored ad hoc to show explosive phenomena and the system displays the transitions under changes in a global control parameter (the coupling strength), unlike the explosive percolation which is induced locally, by adding or removing single links. Also, it is well established that dynamical and structural correlations are necessary to induce the explosive behavior<sup>17,18,23</sup> and recently, it has been suggested that these correlations can be related to maximal global synchrony<sup>31,32</sup>. However, it is not understood how empirical oscillator networks can self-organize toward these explosive regimes, when they usually evolve under uncertain or stochastic conditions and exploit only limited, decentralized information available in the immediate surroundings of the units<sup>5,7,17,33</sup>.

To tackle some of the aforementioned challenges from a theoretical perspective, here we present a self-organized dynamical network that act as a synchronization bomb, i.e. showing an abrupt synchronization transition in the course of a self-organized wiring process. In this way, our model attempts to bridge the conceptual gap between explosive synchronization and percolation by imposing local structural perturbations instead of global ones and proposes a self-organized route to explosive synchronization by invoking a simple principle of synchrony maximization in a decentralized and stochastic process.

The remainder of this paper is organized as follows. We first present our model of the synchronization bomb for an ensemble of Kuramoto oscillators. We introduce the optimal local rule for connecting or disconnecting units, derived from the truncated expansion of the linearized dynamics<sup>31</sup> under the assumptions of maximizing global synchrony with local information, and explore the basic mechanisms and phenomenology of the synchrony-driven percolation process. Second, we analyze the explosive fingerprints that emerge on the underlying structure, in the form of degree-frequency correlations, disassortative dynamical and structural patterns, and a delayed percolation threshold. Third, we provide an analytical characterization of the dynamics by means of the Collective Coordinates<sup>34,35</sup> (CC) and Ott-Antonsen<sup>36</sup> (OA) model reduction techniques, unveiling the dependence of the main parameters and observing an excellent agreement with numerical simulations. Next, we extend the model to numerically produce synchronization bombs of coupled chaotic Rössler systems and cardiac pacemaker cells. We conclude with a discussion of our Results and a Methods' section, including the mathematical machinery used to derive the local rule and the analytical predictions for the percolation and synchronization critical thresholds.

In the Supplementary Information, we study the robustness of the presented phenomenology under variations in system parameters. In particular, in Supplementary Note 1, we study the effects of size and noisy sampling, showing that the explosive transitions induced by single links are sustained for increasing size and that the presence of some randomness is beneficial because it improves the decentralized optimization of synchrony driven by a local rule. In Supplementary Note 2, we study the effect of different choices of frequency distributions. In Supplementary Note 3, we validate the extension of the model to directed networks, and in Supplementary Note 4, we explore in more detail the relation between percolation and synchronization onsets in the model.

## Results

**Model.** We consider a large system of heterogeneous coupled oscillators on top of a network of interactions that evolves under a

competitive link percolation process<sup>10,17</sup>. For the dynamics, we begin with the classical Kuramoto model, a paradigmatic example of the emergence of collective synchronization<sup>19,20,37</sup>. An ensemble of  $N$  heterogeneous Kuramoto oscillators interacting on top of a network follows the equations of motion:

$$\dot{\theta}_i = \omega_i + \lambda \sum_{j=1}^N a_{ij} \sin(\theta_j - \theta_i), \quad \forall i \in 1, \dots, N, \quad (1)$$

where  $\theta_i$  is the phase and  $\omega_i$  is the intrinsic frequency of the  $i$ -oscillator,  $a_{ij}$  are the entries of the adjacency matrix  $A$ , that capture the interactions among the units and  $\lambda$  is a constant coupling strength. As usual, the macroscopic behavior of the system is captured by the modulus of the Kuramoto order parameter:

$$r(t) = \frac{1}{N} \left| \sum_{j=1}^N e^{i\theta_j(t)} \right|, \quad (2)$$

which measures the degree of phase synchronization and is bounded between zero and one. In the following, we will make use of temporal averages of the order parameter, i.e.  $r = \langle r(t) \rangle$ . Although our results can be extended to more general settings, in the following we restrict our study to the case of unweighted ( $a_{ij} = 0, 1$ ) and undirected networks ( $a_{ij} = a_{ji}$ ), and consider, for analytical convenience, a uniform frequency distribution  $g(\omega) \in [-\gamma, \gamma]$ , shifting the resulting frequency vector to have zero mean.

The growth of the synchronization bomb is made by keeping the coupling strength  $\lambda$  constant and varying the density in the number of connections between the units,  $p$ , that acts as the control parameter and ranges from 0 (disconnected network) to 1 (fully-connected network). In the forward process we initialize our system from scratch, with a completely disconnected network ( $p = 0$ ) of oscillators with assigned random phases drawn from  $(-\pi, \pi)$  (other choices are explored in Supplementary Note 2). We then run the percolation processes in which at each step one new link is added. This way the control parameter  $p$  changes sufficiently slow such that the system in Eq. (1) reaches the stationary state at each network step in the process. The addition of a new link at each  $p$ -step is made as follows: We uniformly sample  $M$  pairs of disconnected oscillators and select the connection  $(i, j)$  that maximizes the gain of synchrony given by:

$$\Delta r_{ij} = \frac{1}{\lambda^2 N} \left( \frac{\omega_i}{k_i} - \frac{\omega_j}{k_j} \right) \left( \frac{\omega_i}{k_i^2} - \frac{\omega_j}{k_j^2} \right). \quad (3)$$

In practice, when connecting isolated nodes at the very initial steps of the process, we add an infinitesimal  $\epsilon$  to the degrees of the nodes with  $k_i = 0$  to evaluate Eq. (3) in terms only of the natural frequencies ( $\epsilon = 1$  does not alter the results). In the backward process, we just remove the links in the reversed order of the forward process. The proposed model is stochastic in nature but becomes completely deterministic in the limit  $M \rightarrow \infty$ , and it reduces to the random percolation case in  $M = 1$ .

Equation (3) captures the actual change in the order parameter  $r$  in the strong phase-locking regime (i.e. after the transition) but it can be used to estimate the impact of each link in the whole synchronization process (see Methods section “Derivation of the local rule” for in depth derivation and discussion of this expression). Note that Eq. (3) only exploits local information of the considered nodes, and it is maximum when the ratios frequency-degree of the nodes are large and also when their difference is large as well, pinpointing a clear signature of frequency-degree correlations and frequency-frequency anti-correlations. These correlations were imposed ad hoc in previous models that induce explosive synchronization<sup>17</sup>, and they could indeed emerge from applying a broader class of local percolation

rules in the form  $p(\omega_i, k_i, \omega_j, k_j)$ , but we focus on Eq. (3) since it is the rule that is derived from a decentralized optimization of the phase-locking state, without other assumptions or guesses required.

In Fig. 1a, we illustrate the former basic mechanics for assigning a link out of  $M = 5$  possible candidates and in Fig. 1b we show the histogram of the values of Eq. (3) for all the existing links at a given step of the process, highlighting the value of the five sampled, potential new links. We take the forward process (construction of the network by adding links) as an example. As shown in Fig. 1a the functional form of the basic rule, Eq. (3), induces some relevant features on the interplay between structural and dynamical patterns during the network growth. We observe that nodes with large (small) absolute frequencies accumulate more (less) neighbors, whereas links tend to be more present between nodes with alternate frequencies, producing bipartite-like structures, as we will explore in the following lines. In Fig. 1c we show the forward and backward explosive synchronization transitions by plotting the curves  $r(p)$  when different values of  $M$  are used. We observe that as  $M$  increases so it does the abruptness of the transition as well as the hysteresis region. To illustrate better the explosive nature of these transitions we show in Fig. 1d, e the transition from incoherence ( $r \approx 0.05$ ) to full phase-locking ( $r \approx 0.9$ ) when a unique link is added to the system (in Supplementary Note 1 we check that this effect holds for larger sizes). This phenomenon motivates our choice for referring to these growing networks as synchronization bombs.

**Structural explosive fingerprints.** Before characterizing the synchronization transition of explosive bombs in more depth, we now focus on the structural changes that the network undergoes during the percolation process governed by Eq. (3). In the following we analyze the emergence of several structural and dynamical patterns that are usually associated with explosive transitions<sup>17,31</sup>.

*Degree-frequency correlations and frequency-frequency anticorrelations.* During the network growth process, the system tends to a stationary degree distribution (which scales with system density) as sampling increases in the process (for larger  $M$ ). To understand this effect, we recall that the rule of Eq. (3) tends to connect pairs of oscillators with large frequency differences and low degrees. When a link is chosen, the degrees of the adjacent nodes increase, reducing the value of  $\Delta r_{ij}$  for other potential links of these nodes. This constant competition between fixed frequencies and evolving degrees acts as a self-organized feedback that tends to homogenize the distribution of  $\Delta r_{ij}$  among the potential links, and frequencies and degrees become balanced in the precise way that makes  $\Delta r_{ij}$  more similar among these—still absent—links. Since the rule predicts the scaling  $\Delta r \sim \omega^2/k^3$ , we find that, in the deterministic (large  $M$ ) regime (see Methods section for details) the relation is given by:

$$k_i \approx \frac{5}{3} p N \gamma^{-2/3} |\omega_i|^{2/3}, \quad (4)$$

where the scaling is controlled by the mean degree, expressed in terms of the density of links  $p$  and size  $N$ , since  $\langle k \rangle \approx pN$ . As expected, Eq. (4) becomes more accurate as sampling increases in the system, as observed in Fig. 2a. In Fig. 2b, we see that frequency anti-correlations among pairs of connected nodes are also present in the system and become stronger for large sampling  $M$ . Let us note that these type of correlations are explicitly imposed in the majority of studied mechanisms that induce explosive synchronization<sup>17,18</sup> whereas here emerge from a decentralized optimization of the synchronized state. In the following, we

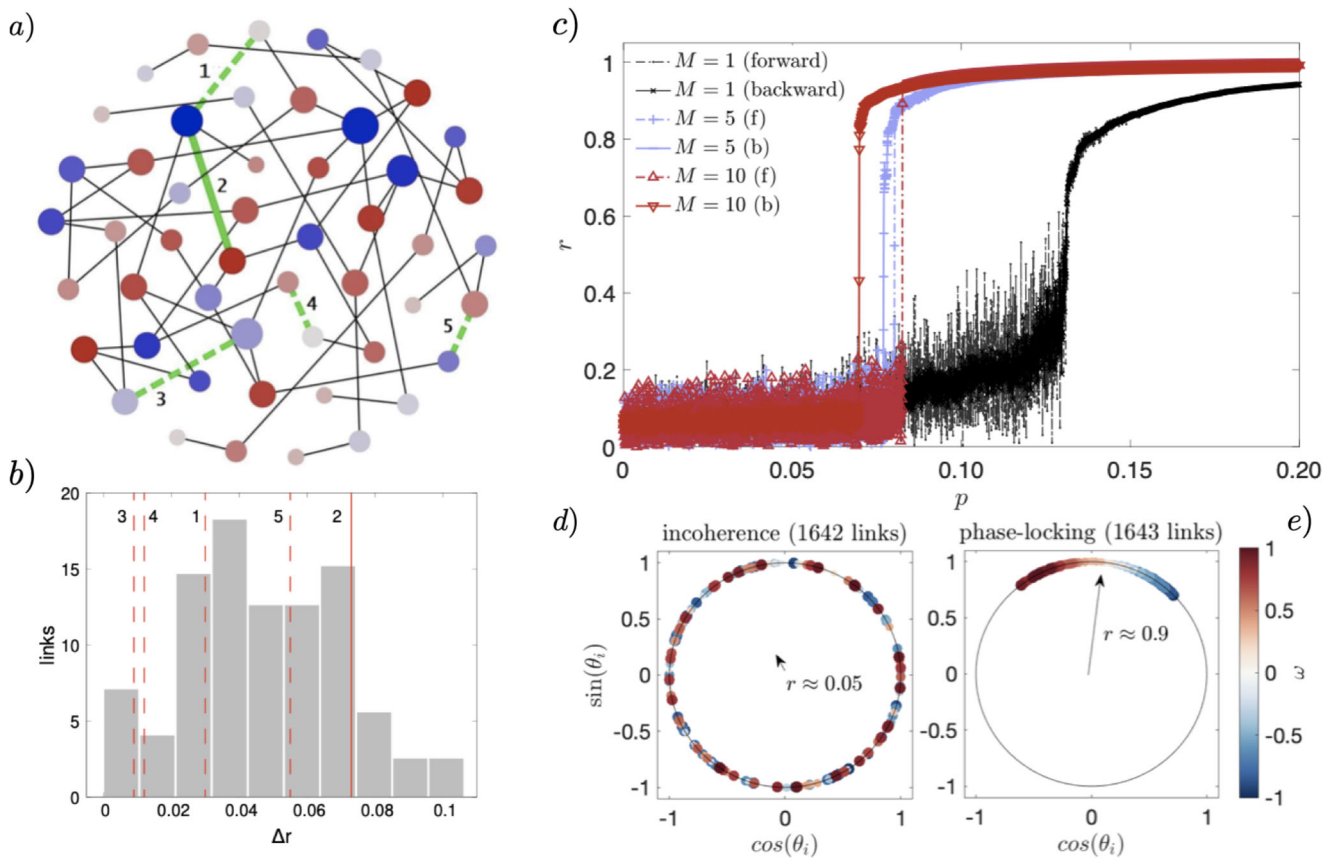


**Fig. 1 Basic phenomenology in the Kuramoto bomb.** **a** Illustrative network of  $N = 50$  oscillators where the size of the node is proportional to its degree, the color is related to its natural frequency (blue for  $\omega = -1$ , gray for  $\omega = 0$  and red for  $\omega = 1$ ) and the black lines represent the links between the oscillators. Green lines mark the  $M = 5$  potential links sampled in that  $p$ -step. The continuous line represents the chosen link and the dashed ones are the discarded ones. **b** Histogram of the  $\Delta r$  values for the existing links of the network, where red lines correspond to the values of the five sampled links. **c** Example of the typical synchronization transition in our bomb-like model, with the order parameter  $r$  depending on the fraction of links,  $p$  in a system of  $N = 200$  Kuramoto oscillators for fixed coupling strength  $\lambda = 0.05$  and three values of sampling  $M$ . Equation (1) is numerically integrated using Heun's method, with  $dt = 0.05$ ,  $10^4$  time steps and temporal averages of  $r$  are taken at each link change. In **d**, we represent the oscillators phases for the  $M = 10$  case before and in **e** after the forward transition. Note that this jump in the Kuramoto order parameter from incoherence to complete phase-locking takes place just with the addition of one link.

explain how these dynamical anti-correlations translate into structural ones.

**Spectral signatures: toward optimal and bipartite networks.** We study the evolution of the extreme eigenvalues  $\mu_{\max}$  and  $\mu_{\min}$  of the Laplacian matrix  $L = D - A$  ( $D$  is the diagonal matrix of degrees) and of the normalized Adjacency matrix  $\hat{A} = D^{-\frac{1}{2}}AD^{-\frac{1}{2}}$  during the percolation process, for different values of sampling  $M$ . In Fig. 2c, d, we observe that the network evolves in a path that maximizes both the largest positive eigenvalue of  $L$ ,  $\mu_{\max}(L)$ , ranging from zero to  $N$ , and the largest negative eigenvalue of  $\hat{A}$ ,  $\mu_{\min}(\hat{A})$ , ranging from minus one to zero, when randomness is reduced in the process (larger sampling  $M$ ). Also, the frequency of the oscillators tends to correlate with the entries of the associated extreme eigenvectors (see insets of both panels). These spectral signatures pinpoint that our model evolve toward optimal and bipartite configurations. First, it is well understood that optimal synchronization is achieved by the alignment of the frequencies with the largest eigenvector of the Laplacian matrix and by increasing the magnitude of the associated eigenvalue  $\mu_{\max}(L)$ <sup>38</sup>. Second, note that the normalized Adjacency matrix,  $\hat{A}$ , is a stochastic row sum and its spectra is bounded in  $\mu(\hat{A}) \in [-1, 1]$ , with the largest eigenvalue  $\mu_{\max}(\hat{A}) = 1$  if the

network is connected. The remaining of the spectra follows Wigner's semicircle law for random networks, becoming narrower as the link density increases, and it deviates from the random case in the presence of modules (shifting toward positive eigenvalues) or bipartite-like structures (shifting toward negative eigenvalues)<sup>31</sup>. Thus, from Fig. 2d we observe that bipartite patterns arise as determinism is increased (larger  $M$ ) and the trajectory of the extreme eigenvalues tuple follows a clear asymmetric path toward the all-to-all ( $p = 1$ ) limit. This effect shows that the rule derived in Eq. (3) induces negative structural correlations (bipartitivity) as a consequence of the negative dynamical correlations that emerge in terms of natural frequencies, and vice-versa.

**Delayed percolation threshold.** From the former results, it is clear that, as the percolation process evolves, the network self-organizes its architecture according to well-known explosive patterns. Two main issues are how this synchrony-driven percolation is related to the natural one, i.e. that observed when links are chosen at random, and, as we will cover below, how the emergence of a giant component (the proportion of the nodes connected in the largest cluster of the network) is related to the synchronization onset. To address these issues we study the emergence of the giant component as a function of the control

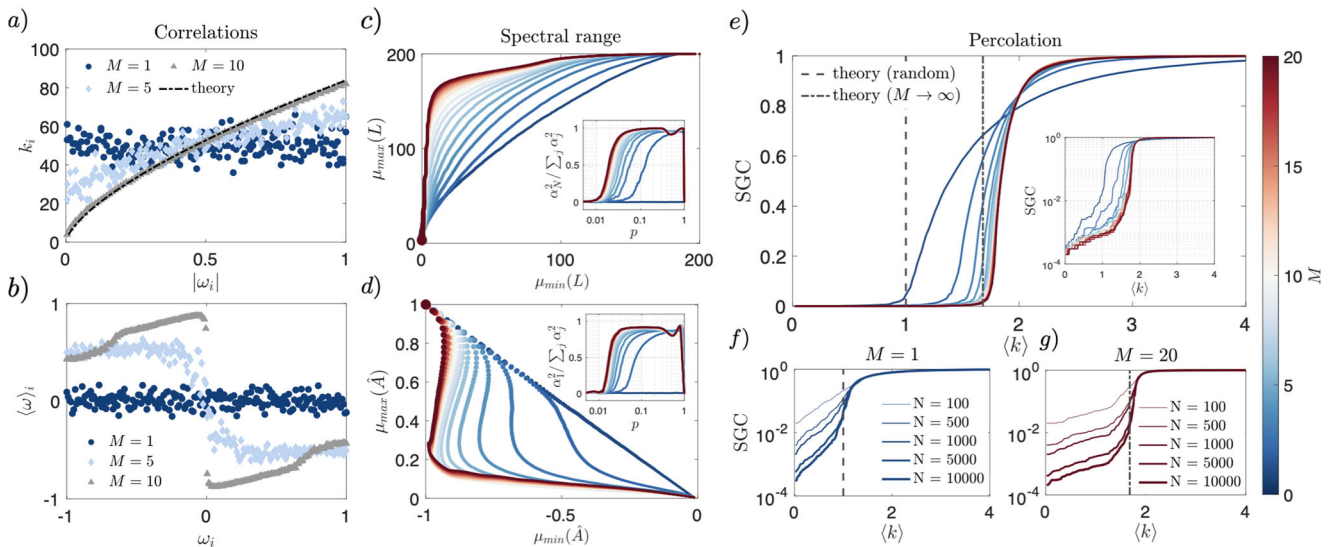


**Fig. 2 Explosive fingerprints.** Left column: **a** scatter plot of the tuples  $(|\omega_i|, k_i)$  and **b**  $(\omega_i, \langle \omega \rangle_i)$ —where  $\langle \omega \rangle_i$  is the average frequency of the neighbors of the  $i$ th-node—for each oscillator at  $p = 0.1$ , in a single realization of the forward process, for three values of sampling and  $N = 200$ , including in **a** the deterministic prediction of Eq. (4). Middle column: scatter plot of **c** the maximum and minimum eigenvalues of the Laplacian matrix,  $\mu_{\min}(L)$  and  $\mu_{\max}(L)$  and **d** of the normalized Adjacency matrix,  $\mu_{\min}(\hat{A})$  and  $\mu_{\max}(\hat{A})$  at different  $p$ -steps of the forward process (the size of the dots decreases for larger  $p$ ) for different values of  $M$ . In the inset, we plot the relative correlation  $\alpha_i = \langle \omega_i, v_i \rangle$  between the frequency vector and the eigenvector of  $L$  (or  $\hat{A}$ ) associated with the maximum (or minimum) eigenvalue. Right column: **e** Evolution of the average size of giant component (SGC), for sampling ranging from the random scenario of  $(M = 1)$  to a more deterministic one with  $(M = 20)$  in a network of size  $N = 5000$ . Results are averaged over 20 realizations of the process. Inset in **e** shows a single realization in log scale. In **f** we show the effect of network size on the percolation transition for the  $M = 1$  and **g**  $M = 20$  scenarios. It is observed that larger and more deterministic networks under the rule of Eq. (3) experiment sharper transitions.

parameter  $p$  when the rule of Eq. (3) is applied for different values of the sampling parameter  $M$ . In Fig. 2e, we observe that the proposed rule delays the percolation threshold with respect to the random case, and it produces more abrupt transitions. Looking more closely at the effect of the system parameters on the percolation threshold, in Fig. 2f, g we observe that, when increasing both the size of the system (large  $N$ ) and the determinism in the rule (large  $M$ ), percolation transitions become sharper and occur at higher  $p$ . Nevertheless, the nature of the transition appears to be continuous (*i.e.* second order) even for large system sizes. We can obtain a rough approximation for the average value of the percolation threshold by using the well-known Molloy and Reed criterion<sup>39</sup> in the deterministic limit and neglecting the negative structural correlations that the rule induces. Using this criterion and leveraging the emergent degree-frequency correlation we obtain, for a uniform  $g(\omega)$ , (see Methods) that the threshold is estimated as:

$$p_c = \frac{42}{25N}, \tag{5}$$

which can be written in terms of the percolation threshold in a random network<sup>9</sup> as  $p_c \approx 1.68 \cdot p_c^{rand}$ . In Fig. 2e we observe that Eq. (5) works quite well for sufficiently large  $M$ . More sophisticated analytical tools, as the recently developed feature-enriched percolation framework<sup>40</sup>, could improve the predictions under local rules, such as Eq. (3), that exploit information both from the degrees and the frequencies of the units.

**Analytical characterization of the Kuramoto bomb.** Now we explore, by analytical and numerical means, the dynamical regimes of our system depending on the coupling,  $\lambda$ , and sampling,  $M$ , values. We remark that, despite the apparent simplicity of Eq. (1), the Kuramoto Model on complex networks does not have an analytical solution and approximations are required to

predict the dynamical behavior using the information contained in  $A$  and  $\omega$ <sup>17,20</sup>.

To the best of our knowledge, the current method that better captures the finite-size effects and the precise interplay between the structure and the oscillator dynamics in Eq. (1) is the model reduction technique based on Collective Coordinates, introduced first by Gottwald to globally coupled systems<sup>34</sup> and extended to complex networks in<sup>35</sup>. We use this approach to estimate the value of the oscillator phases and the corresponding evolution of the order parameter  $r(p)$  in the backward branch and also to calculate numerically the backward synchronization threshold,  $p_c^b$ . See Methods section “Collective coordinates ansatz” for the precise details of this method. The agreement between CC theory and numerical simulations becomes evident in the backward synchronization diagrams shown in Fig. 3a for  $\lambda = 0.02$  and  $0.04$  ( $M = 10$ ).

For the forward process we cannot use the CC approach and we rely on the celebrated OA ansatz<sup>36</sup>, which has been successfully used to characterize systems in the presence of frequency and degree correlations<sup>41–43</sup>. Specifically, we benefit from a recent elegant development used to describe the mean-field dynamics of Janus oscillators<sup>43</sup> and consider the limit of large  $N$  and  $M$ . Complete calculations to predict the loss of stability of the incoherent state, and therefore the forward synchronization threshold, are given in the Methods section “Ott-Antonsen ansatz”. For the particular case of a uniform distribution  $g(\omega) \in [-1, 1]$  we obtain the closed form:

$$p_c^f \approx \frac{21}{25\lambda N}. \tag{6}$$

The predicted value  $p_c^f$  is plotted in Fig. 3a showing again a remarkable agreement. This analytical estimation allows addressing the aforementioned issue about the relation between synchronization and percolation onsets by making use of Eqs.

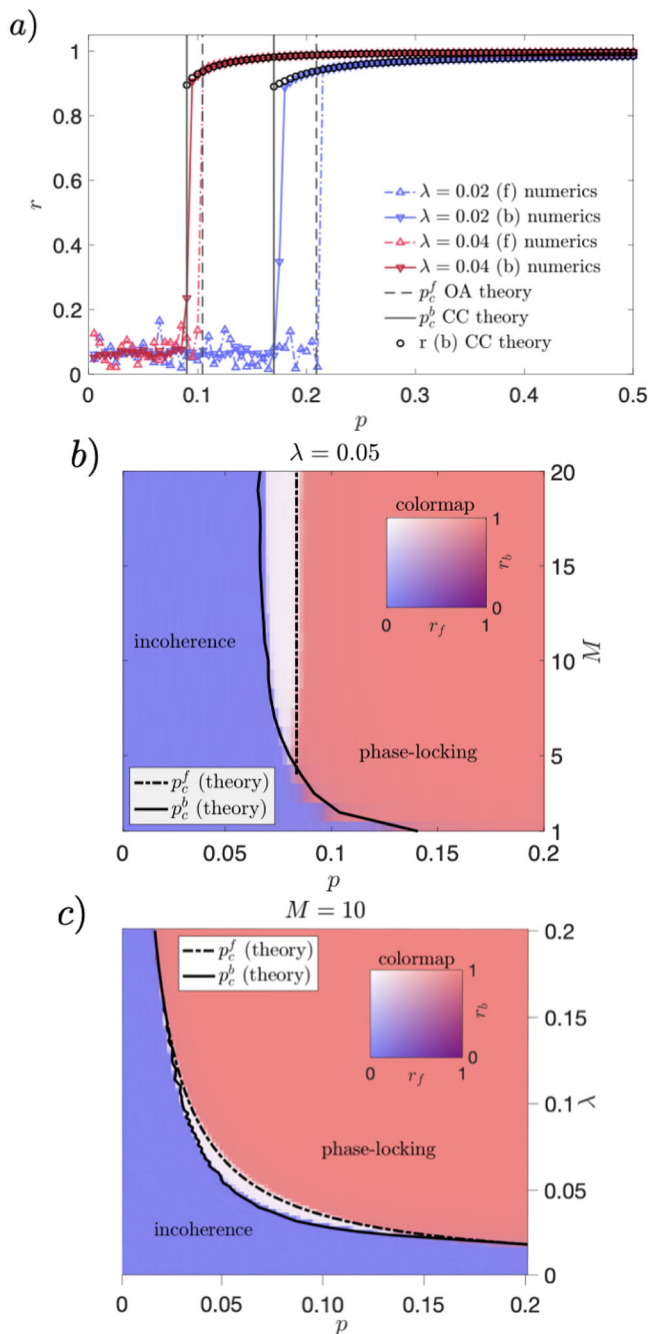


**Fig. 3 Analytical characterization of the Kuramoto bomb.** **a** Two examples of synchronization curves,  $r(p)$  in the forward and backward processes, for a rule dependent ( $M = 10$ ) case in a network of size  $N = 200$  and fixed coupling to  $\lambda = 0.02$  and  $\lambda = 0.04$ . Measurements here are taken every 40 links and results are obtained in a single realization of the process.

**b** Synchronization phase-space depending on  $M$  and  $p$  for a fixed  $\lambda = 0.05$ . In the three panels, dashed (solid) lines correspond to the theoretical predictions of the forward (backward) synchronization thresholds, and circle markers in **a** give the analytical prediction of the whole backward curve (see main text and Methods section for the derivations). Note that the results displayed in Fig. 1c correspond to three  $M$  – slices here.

**c** Synchronization phase-space depending on  $\lambda$  and  $p$  for a certain level of sampling  $M = 10$ . The color in the two-dimensional colormap indicates the numerical values of the tuple  $(r_f, r_b)$ , and shows that the system is either in the incoherent (purple), bistable (white) or full phase-locking regime (red). Results are averaged over 20 realizations.

(5) and (6). Combining both expressions we can write a simple relation for the percolation  $p_c$  and forward synchronization  $p_c^f$  thresholds as:

$$p_c \approx 2\lambda p_c^f, \quad (7)$$

which illustrates the natural connection between the structural and dynamical aspects of our model.

We extend our numerical and analytical characterization of the synchronization diagram in the  $(p, M)$ -plane, Fig. 3b), and  $(p, \lambda)$ -plane, Fig. 3c). In Fig. 3b, we observe that, fixing  $\lambda = 0.05$ , the collision of the theoretical backward curve and the approximated forward threshold successfully predicts the codimension-two point, where a saddle-node bifurcation collides with a pitchfork bifurcation and bistability emerges<sup>29</sup>. This critical point for which explosive behavior shows up takes place around  $M \approx 5$ . In Fig. 3c, we focus on the coupling strength  $\lambda$ , a parameter that does not play a role in the percolation process, but it is crucial to synchronization dynamics. The precise location of the synchronization thresholds can be controlled from occurring simultaneously with the percolation one for large values of  $\lambda$  (where the oscillators immediately synchronize when connected and the synchronization curves follow the percolation ones shown in Fig. 2e), to occur much later for smaller values of  $\lambda$  (where bistability and abruptness of transitions is maximized) and to finally disappear for sufficiently small  $\lambda$ . Interestingly, in the explosive range of  $\lambda$ , the emergence of a bipartite structure for sufficiently large  $M$ —as discussed in the previous section—hinders the formation and growth of microscopic small clusters in the incoherent regime (see for instance Fig. 1d), against what occurs in other models of explosive synchronization<sup>17,23,30</sup>. Furthermore, we note that the system transits more abruptly for a relatively large  $\lambda$  (low  $p$ ), but has a larger region of hysteresis for low  $\lambda$  (large  $p$ ).

In Supplementary Note 1 we explore the dynamics of the model for different system sizes, confirming that the abrupt jump in  $r$  occurring at single link changes remains large for increasing size, and we analyze in more detail the role of the noisy sampling in the model, finding that an optimal amount of sampling can enhance the explosive performance of the synchronization bomb because it improves the self-organized optimization process driven by a local rule. In Supplementary Note 2 we show that both phenomenology and theory are robust to changes in the distribution of intrinsic frequencies,  $g(\omega)$ . In particular, we show results for Gaussian (and bimodal) cases, exploring scenarios with less (and more) polarization than the uniform distribution, finding the expected result that polarization in  $g(\omega)$  increases the bistable regime and the abruptness of the transitions. In Supplementary Note 3 we show that the bomb-like transitions also occur for directed networks. Lastly, in Supplementary Note 4 we also illustrate in more detail the relation between percolation and synchronization curves under the parametrization of Fig. 3c.

**Chaotic synchronization bombs.** One of the most relevant applications of synchronization theory is its implementation when coupling chaotic systems<sup>44</sup>, a counter-intuitive non-linear phenomenon as it achieves a perfect dynamical coherence between systems that, when isolated, display exponential divergence of nearby trajectories. Thus, to show the generality of our results, we round off by extending them beyond the Kuramoto framework and considering the Rössler system, a paradigmatic model for the emergence of chaotic dynamics<sup>45</sup>.

Here we use an ensemble of diffusively coupled heterogeneous chaotic oscillators<sup>46–48</sup>, a modified, piece-wise linear Rössler

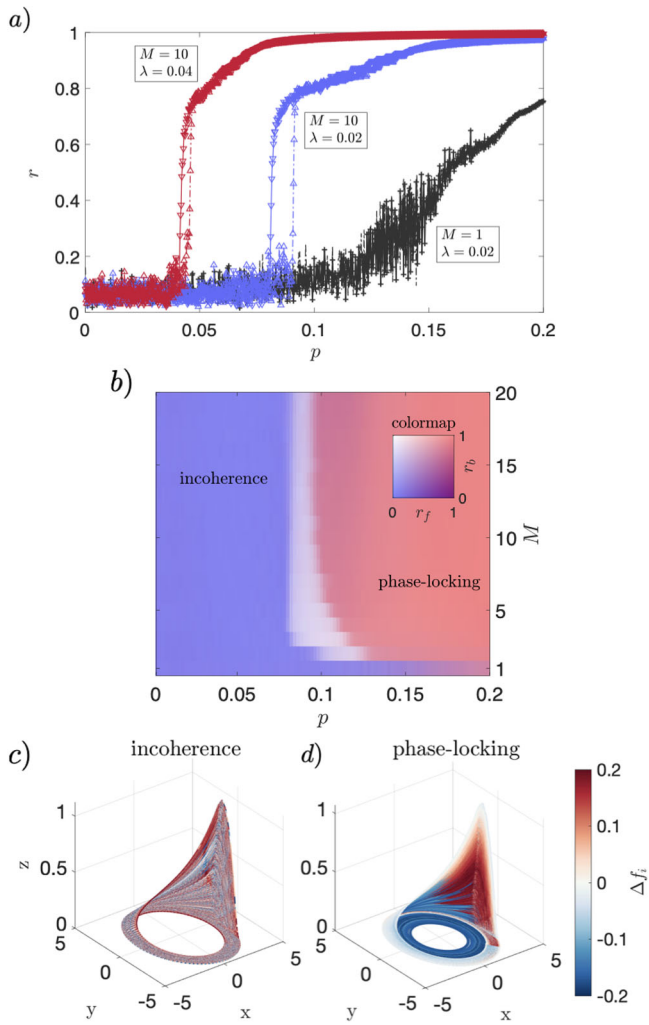


**Fig. 4 Chaotic synchronization bombs.** **a** Example of synchronization curves for several values of  $M$  and  $\lambda$ . It is observed that a hysteresis cycle appears when  $M > 1$  and that lower (higher) values of  $\lambda$  translate into wider (more narrow) cycles and less (more) abrupt transitions. **b** Synchronization phase-space, depending on  $p$  and  $M$  for a fixed  $\lambda = 0.02$ . Results are qualitatively similar to the ones found in Fig. 3b, although here the transitions are less abrupt and narrower than in the Kuramoto case, and the birth of hysteresis occurs for lower sampling (lower  $M$ ). **c** Evolution of the oscillators trajectories in the Rössler attractor for  $M = 10$  and  $\lambda = 0.02$  at two different  $p$ -steps, before and **d** after the forward synchronization transition. The color bar corresponds to the frequency of the oscillator relative to the mean. Equation (8) is numerically integrated using Heun’s method, with  $dt = 0.05$  and  $10^3$  time steps and temporal averages of  $r$  are taken at every 5 link changes.

system<sup>45</sup>, which evolves in a 3-dimensional space following:

$$\begin{aligned} \dot{x}_i &= -f_i \left[ \tau \left( x_i - \lambda \sum_{j=1}^N a_{ij}(x_j - x_i) \right) + \beta y_i + \delta z_i \right], \\ \dot{y}_i &= -f_i(-x_i + \nu y_i), \\ \dot{z}_i &= -f_i(-g(x_i) + z_i), \end{aligned} \tag{8}$$

where the non-linear function that induces the chaotic behavior is defined as  $g(x) = 0$  if  $x \leq 3$  and  $g(x) = \mu(x - 3)$  if  $x > 3$ . The remaining parameters are set following<sup>47,48</sup>, with  $\tau = 0.05$ ,  $\beta = 0.5$ ,  $\delta = 1$ ,  $\nu = 0.02 - 100/R$ .  $R = 100$  ensures that the system is in a phase-coherent regime<sup>46–48</sup>, where a phase can be defined after projecting onto the  $xy$ -plane, i.e.  $\theta_i = \arctan(y_i/x_i)$ , such that

the synchronization order parameter  $r$  can be measured by the standard Eq. (2). See Fig. 4c, d for a 3D representation of the trajectories of the chaotic, phase-coherent, oscillators at two different  $p$ -steps of the forward process. As in Eq. (1),  $\lambda$  is the fixed coupling strength and the entries  $a_{ij}$  of the adjacency matrix  $A$  capture the presence of undirected and symmetric interactions between the oscillators and evolve under the rule of Eq. (3). The instantaneous velocity of each unit is determined by  $f_i$ , which we assign proportional to the frequency,  $f_i = 10 + 0.2\omega_i$ , drawn again from a uniform distribution  $g(\omega)$  in  $[-1, 1]$ .

Figure 4a illustrates three examples of synchronization transitions  $r(p)$  for a system of  $N = 200$  and different choices of  $\lambda$  and  $M$ . Similarly to the Kuramoto case, it is observed how, in the construction process, for sampling values of  $M > 1$  the order parameter experiments abrupt jumps from dynamical incoherence of  $r \sim 0.1$  to a more coherent state with  $r \approx 0.7$ , that continues to continuously grow to stronger synchronization ( $r \gtrsim 0.9$ ) as the link fraction,  $p$ , increases. For the backward transition the inverse process takes place but with the jump to incoherence happening for lower values of  $p$ , resulting in a small hysteresis cycle. In Fig. 4c we show the synchronization diagram in the  $(p, M)$ -plane, where it becomes clear that the bistable region shows up even for very small values of  $M$ .

The success of the chaotic synchronization bomb is grounded on previous research that exploits optimal<sup>48</sup> and explosive<sup>47</sup> synchronization properties of the Kuramoto Model on the diffusively coupled Rössler system. However, as numerical results in Fig. 4a, b manifest, the phenomenology is slightly noisier than in the Kuramoto case and the tuning of more parameters along with the chaotic behavior of the units may difficult its design and control. From a practical standpoint, these results show that synchronization bombs could be potentially implemented in the lab, at least by means of electronic circuits<sup>47</sup>.

**Application to cardiac pacemaker cells.** Lastly, we demonstrate the existence of self-organized explosive synchronization bombs in the biologically-plausible application of cardiac pacemaker cells—the collection of cells responsible for generating a strong, coherent pulse that propagates through the entire heart and initiates each contraction<sup>49</sup>. For simplicity, we consider a system of network-coupled pacemaker cells using, for each pacemaker, a two-variable system describing the dimensionless trans-membrane voltage  $v$  and gating variable  $h$  which summarizes ionic concentrations<sup>49</sup>. For a system of  $N$  such pacemakers the equations of motion are given by:

$$\dot{v}_i = \tau_i^{-1} f(v_i, h_i) + K_v \sum_{j=1}^N a_{ij}(v_j - v_i), \tag{9}$$

$$\dot{h}_i = \tau_i^{-1} g(v_i, h_i) + K_h \sum_{j=1}^N a_{ij}(h_j - h_i), \tag{10}$$

where the local dynamics of  $v_i$  and  $h_i$  are described by:

$$f(v, h) = \frac{h(v + 0.2)^2(1 - v)}{0.3} - \frac{v}{6}, \tag{11}$$

$$\begin{aligned} g(v, h) &= \frac{1}{150} + (8.333 \times 10^{-4})[1 - \text{sgn}(v - 0.13)] \\ &\times \{0.5[1 - \text{sgn}(v - 0.13)] - h\}. \end{aligned} \tag{12}$$

The timescales  $\tau_i$  represent local heterogeneity between the different pacemakers, scaling the period of each isolated cell, ultimately resulting in an effective natural frequency for each pacemaker proportional to  $\tau_i^{-1}$ . Taking a system of  $N = 200$  pacemakers with  $\tau_i^{-1}$  uniformly distributed in  $[0.4, 1.6]$  and using coupling strengths  $K_v = 0.009$  and  $K_h = 0.0044$  (to indicate a stronger coupling via the voltage diffusion compared to ionic diffusion) we implement the

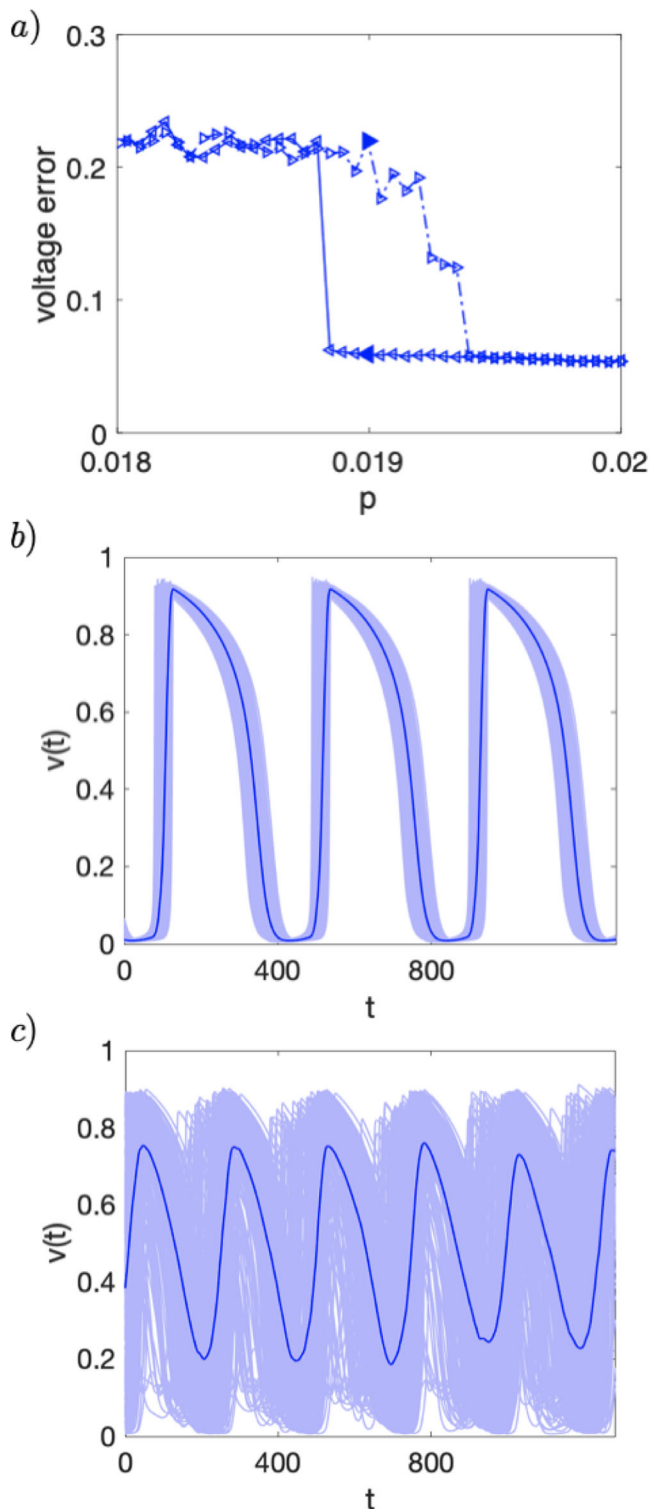


**Fig. 5 Application to a model of cardiac pacemaker cells.** **a** Voltage error (quantified by the standard deviation) as a function of the percolation parameter  $p$ , under forward and backward percolation dynamics plotted in dot-dashed and solid lines, respectively. **b**, **c** Individual voltage time series  $v_i(t)$  and the mean, plotted in light and dark blue strokes, respectively, from right before and after the backward explosive transition.

coupled percolation and synchronization dynamics as presented previously in this work.

To measure the synchronization of the full system we consider the error in the voltage dynamics, quantified by the overall

standard deviation. Taking temporal means of the error as the percolation dynamics are run forward and backwards, we plot the voltage error in Fig. 5a. In Fig. 5b, c we present the actual voltage dynamics right before and after the backward explosive transition, plotting each individual voltage time series  $v_i(t)$  in a light blue stroke, and indicating the overall mean using a thick, dark blue stroke. Note here the physiological implications of the pacemakers ability or inability to produce a strong, coherent pulse for strongly and weakly synchronized behavior, respectively.

By inspecting Fig. 5a, we observe a region of bistability and explosive transitions in the voltage error, being more abrupt in the backward direction, where the transition occurs at a single link removal. As occurred with Rössler dynamics, results are noisier than in the Kuramoto case and the precise location of the thresholds—and the associated width of hysteresis—vary across realizations, presumably due to the small network size considered here. A detailed exploration of the synchronization bombs in these more nuanced oscillator models remains open for further research, but current results already confirm that the main phenomenology is sustained beyond systems of Kuramoto-like phase oscillators.

## Discussion

Abrupt and explosive phenomena in the structure and dynamics of complex networks have been one of the most studied phenomena in non-equilibrium statistical physics and non-linear dynamics in recent years. Not only do they allow us to further our theoretical understanding of phase transitions, but also to develop models that are able to explain and reproduce the changes in the topology and behavior observed in natural and engineered systems, such as biological switches, brain activity and blackouts in power-grids. Motivated by the wide range of applications, network percolation and collective synchronization have become paradigmatic frameworks to understand the explosive changes in the structural and dynamical macroscopic properties of large complex systems. A crucial feature of explosive percolation is that it is induced by applying small localized structural perturbations to the system (addition or removal of a few links) by means of competitive rules that delay the formation of a connected component. This aspect was not explored in the synchronization counterpart, where explosive transitions were usually studied by fine-tuning of global coupling parameters in fixed or evolving structures. Furthermore, while the specific theoretical requirements for the explosive behavior become better understood, there is less knowledge on the actual routes that real systems may follow to self-organize toward these particular configurations.

In this work, we have attempted to bridge these gaps by deriving a local percolation rule for systems of heterogeneous phase-oscillators under the minimal assumption of maximizing global synchronization with decentralized information. We have shown that under this percolation rule the system behaves as a synchronization bomb. This way the network undergoes an explosive synchronization transition at some point of the wiring process, abruptly switching from incoherence to global phase-locking, and display a hysteresis cycle. We have also shown that as the network grows, it self-organizes in a way that several well-known explosive properties on the network structure show up. Crucially, this growth delays the percolation threshold as compared to the usual random case. We have provided an analytical characterization of the system using state-of-art model reduction techniques, obtaining a fair agreement with numerics and being able to reproduce the bistable region in the synchronization phase diagrams. As we show in the SI, all these results are robust under the variation of model assumptions and parameters, and also hold for directed networks. Interestingly, we find that a noisy, low sampling is beneficial in our model because it improves the decentralized optimization of synchrony driven by the proposed local rule. Finally, we

have shown that synchronization bombs can be also obtained for systems of coupled chaotic units, paving the way to their implementation in the lab and in a model of cardiac pacemaker cells, proving potential applications in biological systems.

While the current results provide a self-organized and stochastic route to the emergence of these bombs, alternative, deterministic approaches could lead to a better optimization of the explosive behavior and control of the location of the transitions in empirical networked systems. From a theoretical perspective, our results propose a mechanistic origin of explosive synchronization in phase models, in terms of a local percolation rule that exploits both structural and dynamical information from the degrees and the frequencies of the oscillators. In this sense, our model can be seen as a synchrony-driven process in the recently established framework of feature-enriched percolation<sup>40</sup>. Furthermore, the analytical and numerical findings presented here align well with the novel hypothesis of self-organized bistability in neuronal dynamics<sup>50</sup> and also provide a missing explanation to the emergence of explosive behavior in pair-wise networks via the activation of a single self-organized mechanism, somewhat analogous to the explosive transition described in globally coupled networks when a single parameter, the one controlling the strength of higher-order interactions, is switched on in the system<sup>51</sup>.

In a nutshell, our findings show that growing networks of heterogeneous dynamical units can develop to operate in a bistable regime, forming networked switches that display the dynamical-structural correlations that are observed when graphs are tuned to display explosive behavior. Also, engineered networks can be designed to be at the onset of total synchrony in which they show no dynamical coherence but, after a minimal wiring (just one or few links), experience synchronization explosions. This finding provides a justification for naming these systems as synchronization bombs.

## Methods

**Derivation of the local rule.** We begin with two key assumptions: (1) the system attempts to maximize the overall degree of synchronization, by adding or removing undirected connections in a percolation process and (2) only limited information is available, making this percolation a decentralized process. This means that the units have access only to their immediate surroundings and they can exploit only local information to maximize synchronization, without having access to the overall network synchronization. In order to derive the rule under the previous assumptions, we invoke linearization arguments on the original system Eq. (1), which are shown to be valid when looking for optimal structural and dynamical properties even far away from the linearized regime<sup>38,52</sup>. Under the linearization, the resulting system reads in matrix form as:

$$\dot{\theta} = \omega - \lambda L\theta, \tag{13}$$

where  $L = D - A$  is the Laplacian of the network. The solution of Eq. (13) in the stationary state is found by setting  $\dot{\theta} = 0$ . In the corotating frame at speed  $\langle \omega \rangle = 0$ , the solution reads as:

$$\theta^* \approx \frac{1}{\lambda} L^\dagger \omega, \tag{14}$$

where  $L^\dagger$  is the Moore-Penrose pseudoinverse of the Laplacian matrix, which can be constructed via the spectral decomposition of  $L$  for undirected networks (see ref. <sup>38</sup> for more details). Since we are close to the synchronization attractor, the phases in Eq. (2) can also be expressed in a Taylor expansion<sup>38</sup>. Invoking again linearization, the order parameter is given by:

$$r \approx 1 - \|\theta\|^2 / 2N. \tag{15}$$

In principle, one needs all the spectral information of the network to estimate the value of  $r$ . However, we can leverage recent results on the geometric expansion of Eq. (14)<sup>31</sup>, where it is shown that the linearized solution can be expressed as a sum of contributions from increasingly further neighborhoods. This way, the local approximation of synchrony<sup>31</sup> is obtained by truncating the expansion at its second term (taking into account the effect of the nearest neighbors of the nodes), leading to:

$$r \approx 1 - \frac{1}{2\lambda^2 N} \sum_{i=1}^N \left( \frac{\omega_i + z_i}{k_i} \right)^2, \tag{16}$$

where  $z_i = \sum_{j=1}^N a_{ij}(\omega_j/k_j)$  is the contribution of first neighbors. For more details on the accuracy of Eq. (16), see ref. <sup>31</sup>. From Eq. (16), we can estimate the local impact in the synchrony of adding or removing a single link between oscillators  $(i, j)$ . Both discrete (considering single link perturbations) and continuous (using derivatives with respect to the degrees and the approximation  $\partial z_i / \partial k_n \approx \pm \delta_{ni} \omega_n / k_n$ , evaluating the resulting expression at  $z_i = 0$ ) calculations, in the limit of large degree, lead to Eq. (3) in the results section, an expression that depends only on the local variables  $(\omega_i, k_i)$  of a given pair of nodes. Explicitly:

$$\Delta r_{ij} = \frac{\pm 1}{\lambda^2 N} \left( \frac{\omega_i}{k_i} - \frac{\omega_j}{k_j} \right) \left( \frac{\omega_i}{k_i^2} - \frac{\omega_j}{k_j^2} \right), \tag{17}$$

where the  $\pm$  sign accounts for the addition (removal) of a link. We remark that this result is derived assuming no bias in the coupling function of Eq. (1), symmetric and unweighted interactions and a frequency distribution of zero mean, meaning that the actual frequencies of the oscillators may need an appropriate shift to satisfy the condition<sup>31</sup>. Also, note that one could obtain more accurate rules for the maximization of  $r$  by using the exact result for the phases given by Eq. (14) or by including higher-order terms beyond the local approximation, although this increase of accuracy would require to use either spectral (thus global) information or to go beyond the local variables up to second-neighbors and so on. Furthermore, we note that a quadratic approximation of Eq. (17) as  $\Delta r \sim (\omega_i/k_i - \omega_j/k_j)^2$  also induces the explosive phenomena and may simplify the analytical treatment, but its study is left for further research.

**Derivation of the percolation threshold.** The percolation threshold is approximated by the Molloy and Reed criterion<sup>39</sup>, that predicts the transition for random network without correlations for the value of  $p = p_c$  at which:

$$\langle k^2 \rangle (p_c) = 2 \langle k \rangle (p_c). \tag{18}$$

To compute  $\langle k \rangle$  and  $\langle k^2 \rangle$ , we consider a uniform distribution, such that  $g(\omega) = 1/(2\gamma)$  if  $\omega \in [-\gamma, \gamma]$  (the same analysis could be done for any other frequency distribution) and also take into account that, explicitly, we have the general correlation  $k_i = c|\omega_i|^{2/3}$  where  $c$  is a normalization constant which depends on the network density,  $p$ , as well as the distribution of natural frequencies,  $g(\omega)$ . Using that  $\langle k \rangle = p(N-1)$ , we find that  $c = p(N-1) / \langle |\omega|^{2/3} \rangle$ , with  $\langle |\omega|^{2/3} \rangle = \frac{2}{3} \gamma^{2/3}$ . Thus we obtain the correlation:

$$k_i \approx \frac{5}{3} p N \gamma^{-2/3} |\omega_i|^{2/3}, \tag{19}$$

and with it:

$$\langle k^2 \rangle \approx \frac{25}{9} p^2 N^2 \gamma^{-4/3} \langle |\omega|^{4/3} \rangle = \frac{25}{21} p^2 N^2. \tag{20}$$

Thus, substituting in Eq. (18) we obtain:

$$p_c \approx \frac{42}{25} \cdot \frac{1}{N} = 1.68 \cdot p_c^{rand}, \tag{21}$$

which corresponds to Eq. (5) in the Results section.

**Collective coordinates ansatz.** We use the theory introduced in refs. <sup>34,35</sup> to predict the phases of the oscillators at any given  $p$ -step of the backward process and also the transition from phase-locking to incoherence. The main idea of the method is to reduce the dimensionality of the system by considering, as an *ansatz*, that the phases of the oscillators in the phase-locking regime are in the form:

$$\theta_i = q(t) \psi_i, \tag{22}$$

where  $\psi_i$  is the exact solution of the linearized dynamics of Eq. (1)<sup>38</sup>, i.e.  $\psi_i = \frac{1}{\lambda} L^\dagger \omega$ . By minimizing the error made by Eq. (3) in the full dynamics of Eq. (1) and after some manipulation<sup>35</sup>, one ends up with only one differential equation for the evolution of the  $q$  coefficient, thus drastically reducing the dimensionality from  $N$  coupled differential equations to a single one. The resulting equation reads as:

$$\dot{q} = 1 + \frac{1}{\psi^T L \psi} \sum_{ij} \psi_i \sin(q(\psi_j - \psi_i)). \tag{23}$$

Solving the implicit Eq. (23) for  $\dot{q} = 0$  allows estimating the phases of the oscillators in Eq. (1) beyond the linear regime of the system. Here, we use this theory to predict the phases of the oscillators and the corresponding curve for the order parameter in the full phase-locking regime of the system. Furthermore, to predict the appearance of the (backward) critical threshold  $p_c^b$  within this theory, we use an explosive trick. We assume beforehand that in the explosive regime of our system, the backward process transits from full phase-locking to complete incoherence. With this idea in mind, we predict the backward threshold by looking at the last values  $(p, \lambda)$  for which Eq. (23) has a solution. Additionally, we check that the solution is linearly stable by numerically computing the eigenvalues of the Jacobian matrix of the full system in Eq. (1) around the equilibrium solution  $q = \hat{q}$ . The

Jacobian evaluated at the equilibrium point reads as<sup>35</sup>:

$$\begin{aligned} J_{ij} &= a_{ij} \cos(\hat{q}(\psi_j - \psi_i)), \quad i \neq j \\ J_{ij} &= -\sum_k a_{ik} \cos(\hat{q}(\psi_j - \psi_i)), \quad i = j. \end{aligned} \quad (24)$$

The system is stable if all the eigenvalues of  $J$  are negative. Thus, the backward critical threshold occurs at the last value of  $p_c^b$  at which Eq. (23) admits a solution that is linearly stable. The explosive trick is particularly useful to simplify the calculation because, when considering transitions from full phase-locking to incoherence, we do not need to compute partial synchronized solution involving clusters of smaller size than the whole network<sup>35</sup>. In other words, we predict the loss of stability of the full phase-locking state, which in the explosive regime of our system corresponds to the desired backward synchronization threshold.

**Ott-Antonsen ansatz.** In the forward direction, we cannot use the Collective coordinates approach anymore because our system departs from the incoherent state where the ansatz Eq. (22) is not valid. Numerical simulations showed that, usually for  $M > 1$ , the incoherent state  $r \approx 0$  remains stable beyond the backward critical transition, thus creating a bistable region and a delayed forward transition. In order to analytically predict the forward critical threshold, we consider the limit of large  $N$  and also large  $M$  (toward a deterministic rule). In practice, the following results turn out to be valid even for quite small values such as  $N = 200$  and  $M = 5$ , but we remark that the theory is derived in the infinite size and deterministic limits of the model. Our approach is based on the celebrated OA ansatz<sup>36</sup> and follows a very similar development to that shown in ref. <sup>43</sup>.

We begin by defining the local order parameter:

$$R_i = \sum_j a_{ij} e^{i\theta_j}, \quad (25)$$

such that Eq. (1) can be written as:

$$\dot{\theta}_i = \omega_i + \lambda \text{Im}[e^{i\theta_i} R_i] \quad \forall i \in 1, \dots, N. \quad (26)$$

Following<sup>43</sup>, we consider a large ensemble of systems, described by the joint probability density  $\rho(\theta, \omega, t)$ , with  $\theta = (\theta_1, \dots, \theta_N)$  and  $\omega = (\omega_1, \dots, \omega_N)$ . The evolution of the joint probability has to satisfy the continuity equation<sup>36</sup>:

$$\frac{\partial \rho}{\partial t} + \sum_{i=1}^N \frac{\partial}{\partial \theta_i} (\rho \dot{\theta}_i) = 0. \quad (27)$$

where  $\theta_i$  is given by Eq. (26). Multiplying the density function  $\rho$  by  $\prod_{j \neq i} d\omega_j d\theta_j$  and integrating, one obtains the evolution for the marginal oscillator density,  $\rho_i(\theta_i, \omega_i, t)$  which reads as<sup>43</sup>:

$$\frac{\partial \rho_i}{\partial t} + \frac{\partial}{\partial \theta_i} (\rho_i \dot{\theta}_i) = 0. \quad (28)$$

Now, the OA ansatz can be applied by expanding  $\rho_i$  in a Fourier series and setting the coefficients of the expansion as  $b_{i,n} = \alpha_i^n$ <sup>36,43</sup>. By inserting the Fourier series with the ansatz in Eq. (28), one ends up with:

$$\dot{\alpha}_i + i\alpha_i \omega_i + \frac{\lambda}{2} (\alpha_i^2 R_i - R_i^*) = 0, \quad \forall i \in 1, \dots, N \quad (29)$$

$$R_i = \sum_{j=1}^N a_{ij} \int_{-\infty}^{\infty} \alpha_j^*(\omega_j, t) g(\omega) d\omega_j, \quad \forall i \in 1, \dots, N. \quad (30)$$

where  $R_i^*$  and  $\alpha_j^*$  represent the complex conjugate and  $i$  the imaginary unit. Now we invoke the large  $M$  assumption. In this deterministic limit, the underlying network is purely bipartite, split between nodes with positive frequencies and nodes with negative ones (see the Results section and Fig. 2c, d). Also, in this limit, the frequencies of the oscillators are completely determined by their degrees. Then, we can look for solutions  $\alpha_i = \alpha_{k,\pm}$ <sup>43</sup>, reducing the problem to finding solutions for the coefficients of degree classes in the two groups. The local order parameter in this setting can be written as<sup>43</sup>:

$$R_{k,\pm} = \frac{k}{\langle k \rangle} \sum_{k'} k' p_{k'} \alpha_{k',\pm}^*. \quad (31)$$

The frequencies of the degree classes in the two groups are completely determined by the percolation rule for a wide range of  $p$ , leading to:

$$\omega_{k,\pm} = \pm \left( \frac{k}{c} \right)^{3/2}, \quad (32)$$

where  $c$  is a scaling constant given in Eq. (19). After these considerations, the resulting system can be written as:

$$\begin{aligned} \dot{\alpha}_{k,+} &= -i \left( \frac{k}{c} \right)^{3/2} \alpha_{k,+} \\ &+ \frac{\lambda k}{2 \langle k \rangle} \left[ \sum_{k'} k' p_{k'} \alpha_{k',-} - \alpha_{k',+}^2 - \sum_{k'} k' p_{k'} \alpha_{k',-}^* \right] \end{aligned} \quad (33)$$

$$\begin{aligned} \dot{\alpha}_{k,-} &= +i \left( \frac{k}{c} \right)^{3/2} \alpha_{k,-} \\ &+ \frac{\lambda k}{2 \langle k \rangle} \left[ \sum_{k'} k' p_{k'} \alpha_{k',+} - \alpha_{k',-}^2 - \sum_{k'} k' p_{k'} \alpha_{k',+}^* \right]. \end{aligned} \quad (34)$$

Since we want to evaluate the stability of the incoherent state  $\alpha_{k,\pm} = 0$ , we linearize the system above and evaluate it around  $\alpha_{k,\pm} = \delta \alpha_{k,\pm} \ll 1$ . After neglecting smaller terms of order  $\delta \alpha^2$ , the dependence on the complex conjugates vanish and we are up with the following system for each degree class:

$$\delta \dot{\alpha}_{k,+} = -i \left( \frac{k}{c} \right)^{3/2} \delta \alpha_{k,+} + \frac{\lambda k}{2 \langle k \rangle} \sum_{k'} k' p_{k'} \delta \alpha_{k',-} \quad (35)$$

$$\delta \dot{\alpha}_{k,-} = +i \left( \frac{k}{c} \right)^{3/2} \delta \alpha_{k,-} + \frac{\lambda k}{2 \langle k \rangle} \sum_{k'} k' p_{k'} \delta \alpha_{k',+}. \quad (36)$$

By defining the variables  $\delta x = \sum_{k'} k' p_{k'} \delta \alpha_{k',+}$  and  $\delta y = \sum_{k'} k' p_{k'} \delta \alpha_{k',-}$ , and summing over degree classes (taking into account the degree distribution), we can write:

$$\sum_k k p_k \delta \dot{\alpha}_{k,+} = -i \sum_k \left( \frac{k}{c} \right)^{3/2} k p_k \delta \alpha_{k,+} + \sum_k \frac{\lambda k^2 p_k}{2 \langle k \rangle} \delta y \quad (37)$$

$$\sum_k k p_k \delta \dot{\alpha}_{k,-} = +i \sum_k \left( \frac{k}{c} \right)^{3/2} k p_k \delta \alpha_{k,-} + \sum_k \frac{\lambda k^2 p_k}{2 \langle k \rangle} \delta x. \quad (38)$$

With the approximation  $\sum_k k^{5/2} p_k \delta \alpha_{k,+} \approx \langle k^{3/2} \rangle \delta x$  and  $\sum_k k^{5/2} p_k \delta \alpha_{k,-} \approx \langle k^{3/2} \rangle \delta y$ , the set of equations reduces to a 2-dimensional variational system for the evolution of  $\delta x$  and  $\delta y$  that reads as:

$$\delta \dot{x} = -\frac{i \langle k^{3/2} \rangle}{c^{3/2}} \delta x + \frac{\lambda \langle k^2 \rangle}{2 \langle k \rangle} \delta y \quad (39)$$

$$\delta \dot{y} = \frac{\lambda \langle k^2 \rangle}{2 \langle k \rangle} \delta x + \frac{i \langle k^{3/2} \rangle}{c^{3/2}} \delta y. \quad (40)$$

It is straightforward to show that the critical condition for the stability of the incoherent state is given by:

$$c^{3/2} \lambda \langle k^2 \rangle = 2 \langle k^{3/2} \rangle \langle k \rangle. \quad (41)$$

In particular, the eigenvalues of the Jacobian matrix change from being both imaginary to become both real as density increases in the system. In fact, the fully imaginary spectrum predicts the existence of a center attractor, indicating a marginal stability of the incoherent state. Therefore, one might expect stationary oscillations of the order parameter<sup>43</sup>. Here we do not observe these oscillations in the forward process. The system is initialized with isolated units (in the incoherent state) and remains there as the network evolves in an adiabatic manner. Fortunately, the forward abrupt transition to phase-locking is well predicted by the critical condition given by Eq. (41), when the eigenvalues become real (one positive and one negative) indicating the appearance of an unstable saddle point.

Accordingly, when the condition is achieved in the forward, growth process, the marginal stability of the incoherent state is lost and the system transits to phase-locking.

Using that in the deterministic limit we have that  $k_i = c|\omega_i|^{2/3}$ , and for a general  $g(\omega)$  the constant is given by  $c = \langle k \rangle / \langle |\omega|^{2/3} \rangle$ , we obtain a general closed form for the forward critical threshold ( $p_c, \lambda_c$ ) that is given by:

$$p_c^f = \frac{2 \langle |\omega|^{2/3} \rangle^2 \langle |\omega| \rangle}{\lambda N \langle |\omega|^{4/3} \rangle}. \quad (42)$$

For the particular case of a uniform distribution  $g(\omega) \in [-\gamma, \gamma]$  we can easily compute the expected moments and, after plugging these results in Eq. (42), we end up with the simple formula:

$$p_c^f = \frac{21\gamma}{25AN}. \quad (43)$$

which corresponds to Eq. (6) in the Results section.

### Data availability

Numerical data presented in this work are available from request to the authors.

### Code availability

Computational and visualization codes to reproduce the results of this work are available from request to the authors.

Received: 7 March 2022; Accepted: 13 October 2022;

Published online: 29 October 2022

## References

- Joiner, W. J. et al. Genetic and anatomical basis of the barrier separating wakefulness and anesthetic-induced unresponsiveness. *PLoS Genet.* **9**, e1003605 (2013).
- Kim, M. et al. Functional and topological conditions for explosive synchronization develop in human brain networks with the onset of anesthetic-induced unconsciousness. *Front. Comput. Neurosci.* **10**, 1 (2016).
- Kim, M., Kim, S., Mashour, G. A. & Lee, U. Relationship of topology, multiscale phase synchronization, and state transitions in human brain networks. *Front. Comput. Neurosci.* **11**, 55 (2017).
- Wang, C.-Q., Pumar, A., Garnier, N. B. & Liu, Z.-H. Explosive synchronization enhances selectivity: example of the cochlea. *Front. Phys.* **12**, 1–9 (2017).
- Wang, Z., Tian, C., Dhamala, M. & Liu, Z. A small change in neuronal network topology can induce explosive synchronization transition and activity propagation in the entire network. *Sci. Rep.* **7**, 1–10 (2017).
- Lee, U. et al. Functional brain network mechanism of hypersensitivity in chronic pain. *Sci. Rep.* **8**, 1–11 (2018).
- Chatterjee, A., Kaznessis, Y. N. & Hu, W.-S. Tweaking biological switches through a better understanding of bistability behavior. *Curr. Opin. Biotechnol.* **19**, 475–481 (2008).
- Dobson, I., Carreras, B., Lynch, V. & Newman, D. E. Complex systems analysis of series of blackouts: cascading failure, critical points, and self-organization. *Chaos* **17**, 026103 (2007).
- Newman, M. *Networks: An Introduction*. (Oxford University Press, Inc., 2010).
- Achlioptas, D., D'Souza, R. M. & Spencer, J. Explosive percolation in random networks. *Science* **323**, 1453–1455 (2009).
- De Domenico, M., Granell, C., Porter, M. & Arenas, A. The physics of spreading processes in multilayer networks. *Nat. Phys.* **12** <https://doi.org/10.1038/nphys3865> (2016).
- Bttcher, L., Woolley Meza, O., Araujo, N., Herrmann, H. & Helbing, D. Disease-induced resource constraints can trigger explosive. *Sci. Rep.* **5** <https://doi.org/10.1038/srep16571> (2015).
- Matamalas, J. T., Gómez, S. & Arenas, A. Abrupt phase transition of epidemic spreading in simplicial complexes. *Phys. Rev. Res.* **2**, 012049 (2020).
- Gmez-Gardees, J., Lotero-Vlez, L., Taraskin, S. & Prez-Reche, F. Explosive contagion in networks. *Sci. Rep.* **6**, 19767 (2016).
- Echenique, P., Gómez-Gardeñes, J. & Moreno, Y. Dynamics of jamming transitions in complex networks. *Europhys. Lett.* **71**, 325–331 (2005).
- Lampo, A., Borge-Holthoef, J., Gómez, S. & Solé-Ribalta, A. Multiple abrupt phase transitions in urban transport congestion. *Phys. Rev. Res.* **3**, 013267 (2021).
- D'Souza, R. M., Gmez-Gardees, J., Nagler, J. & Arenas, A. Explosive phenomena in complex networks. *Adv. Phys.* **68**, 123–223 (2019).
- Boccaletti, S. et al. Explosive transitions in complex networks? Structure and dynamics: percolation and synchronization. *Phys. Rep.* **660**, 1–94 (2016).
- Pikovsky, A., Rosenblum, M. G., & Kurths, J. *Synchronization, A Universal Concept in Nonlinear Sciences* (Cambridge University Press, 2001).
- Arenas, A., Diaz-Guilera, A., Kurths, J., Moreno, Y. & Zhou, C. Synchronization in complex networks. *Phys. Rep.* **469**, 93–153 (2008).
- Pazó, D. Thermodynamic limit of the first-order phase transition in the Kuramoto model. *Phys. Rev. E* **72**, 046211 (2005).
- Martens, E. et al. Exact results for the Kuramoto model with a bimodal frequency distribution. *Phys. Rev. E* **79**, 026204 (2009).
- Gómez-Gardeñes, J., Gómez, S., Arenas, A. & Moreno, Y. Explosive synchronization transitions in scale-free networks. *Phys. Rev. Lett.* **106**, 128701 (2011).
- Leyva, I. et al. Explosive transitions to synchronization in networks of phase oscillators. *Sci. Rep.* **3**, 1281 (2013).
- Avalos-Gaytán, V. et al. Emergent explosive synchronization in adaptive complex networks. *Phys. Rev. E* **97**, 042301 (2018).
- Zhang, X., Boccaletti, S., Guan, S. & Liu, Z. Explosive synchronization in adaptive and multilayer networks. *Phys. Rev. Lett.* **114**, 038701 (2015).
- Soriano-Paños, D., Guo, Q., Latora, V. & Gómez-Gardeñes, J. Explosive transitions induced by interdependent contagion-consensus dynamics in multiplex networks. *Phys. Rev. E* **99**, 062311 (2019).
- Skardal, P. S. & Arenas, A. Disorder induces explosive synchronization. *Phys. Rev. E* **89**, 062811 (2014).
- Skardal, P. S. & Arenas, A. Abrupt desynchronization and extensive multistability in globally coupled oscillator simplexes. *Phys. Rev. Lett.* **122**, 248301 (2019).
- Zhang, X., Zou, Y., Boccaletti, S. & Liu, Z. Explosive synchronization as a process of explosive percolation in dynamical phase space. *Sci. Rep.* **4**, 5200 (2014).
- Arola-Fernández, L., Skardal, P. S. & Arenas, A. Geometric unfolding of synchronization dynamics on networks. *Chaos* **31**, 061105 (2021).
- Wei, C., Shengfeng, W., Yueheng, L., Weiqing, L. & Jinghua, X. Explosive synchronization caused by optimizing synchrony of coupled phase oscillators on complex networks. *Eur. Phys. J. B* **94**, eabe3824 (2021).
- Scarpetta, S., Apicella, I., Minati, L. & de Candia, A. Hysteresis, neural avalanches, and critical behavior near a first-order transition of a spiking neural network. *Phys. Rev. E* **97**, 062305 (2018).
- Gottwald, G. Model reduction for networks of coupled oscillators. *Chaos* **25** <https://doi.org/10.1063/1.4921295> (2015).
- Hancock, E. & Gottwald, G. Model reduction for kuramoto models with complex topologies. *Phys. Rev. E* **98** <https://doi.org/10.1103/PhysRevE.98.012307> (2018).
- Ott, E. & Antonsen, T. Low dimensional behavior of large systems of globally coupled oscillators. *Chaos* **18**, 037113 (2008).
- Kuramoto, Y. *Chemical Oscillations, Waves, and Turbulence* (Dover Publications, 2003).
- Skardal, P. S., Taylor, D. & Sun, J. Optimal synchronization of complex networks. *Phys. Rev. Lett.* **113**, 144101 (2014).
- Molloy, M. & Reed, B. A critical point for random graphs with a given degree sequence. *Random Struct. Algorithms* **6**, 161–180 (1995).
- Artime, O. & De Domenico, M. Percolation on feature-enriched interconnected systems. *Nat. Commun.* **12** <https://doi.org/10.1038/s41467-021-22721-z> (2021).
- Restrepo, J. & Ott, E. Mean field theory of assortative networks of phase oscillators. *Europhys. Lett.* **107** <https://doi.org/10.1209/0295-5075/107/60006> (2014).
- Skardal, P. S., Restrepo, J. G. & Ott, E. Frequency assortativity can induce chaos in oscillator networks. *Phys. Rev. E* **91**, 060902 (2015).
- Peron, T., Eroglu, D., Rodrigues, F. & Moreno, Y. Collective dynamics of random janus oscillator networks. *Phys. Rev. Res.* **2** <https://doi.org/10.1103/PhysRevResearch.2.013255> (2020).
- Boccaletti, S., Kurths, J., Osipov, G., Valladares, D. L. & Zhou, C. S. The synchronization of chaotic systems. *Phys. Rep.* **366**, 1–101 (2002).
- Rössler, O. E. An equation for continuous chaos. *Phys. Lett. A* **57**, 397 (1976).
- Rosenblum, M. G., Pikovsky, A. & Kurths, J. Phase synchronization of chaotic oscillators. *Phys. Rev. Lett.* **76**, 1804–1807 (1996).
- Leyva, I. et al. Explosive first-order transition to synchrony in networked chaotic oscillators. *Phys. Rev. Lett.* **108**, 168702 (2012).
- Skardal, P. S., Sevilla-Escoboza, V. P., Vera-Ávila, V. P. & Buldú, J. M. Optimal phase synchronization in networks of phase-coherent chaotic oscillators. *Chaos* **27**, 013111 (2017).
- Djabella, K., Landau, M. & Sorine, M. A two-variable model of cardiac action potential with controlled pacemaker activity and ionic current interpretation, in *2007 46th IEEE Conference on Decision and Control* 5186–5191 <https://doi.org/10.1109/CDC.2007.4434970> (2007).
- Buendía, V., di Santo, S., Villegas, P., Burioni, R. & Muñoz, M. A. Self-organized bistability and its possible relevance for brain dynamics. *Phys. Rev. Res.* **2**, 013318 (2020).
- Kuehn, C. & Bick, C. A universal route to explosive phenomena. *Sci. Adv.* **7**, eabe3824 (2021).
- Dörfler, F., Chertkov, M. & Bullo, F. Synchronization in complex oscillator networks and smart grids. *Proc. Natl. Acad. Sci. USA* **110**, 2005–2010 (2013).

## Acknowledgements

L.A.-F. and A.A. acknowledge the Spanish MINECO (Grant No. PGC2018-094754-B-C2). J.G.-G. acknowledges the Spanish MINECO (Grant No. FIS2017-87519-P), the Departamento de Industria e Innovación del Gobierno de Aragón and Fondo Social Europeo through (Grant No. E36-17R FENOL), and Fundación Ibercaja and Universidad de Zaragoza (Grant No. 224220). A.A. acknowledges financial support from Generalitat de Catalunya (grant No. 2017SGR-896), Universitat Rovira i Virgili (grant No. 2019PFR-URV-B2-41), Generalitat de Catalunya ICREA Academia, and the James S. McDonnell Foundation (grant #220020325). This work was supported by MINECO and FEDER funds through Projects No. FIS2017-87519-P, No. FIS2017-90782-REDT (IBERSINC); from grant PID2020-113582GB-I00 funded by MCIN/AEI/10.13039/501100011033; and by the Departamento de Industria e Innovación del Gobierno de Aragón y Fondo Social Europeo through Grant No. E36-17R (FENOL). S.F.-L. acknowledges financial support by Gobierno de Aragón through the Grant defined in ORDEN IJU/1408/2018. E.-C.B. acknowledges support from the “Agencia Estatal de Investigación” (Ref. PRE2019-088482), Government of Spain (FIS2020-TRANQI; Severo Ochoa CEX2019-000910-S), Fundació Cellex, Fundació Mir-Puig, and Generalitat de Catalunya (CERCA, AGAUR).

## Competing interests

The authors declare no competing interests.

**Additional information**

**Supplementary information** The online version contains supplementary material available at <https://doi.org/10.1038/s42005-022-01039-2>.

**Correspondence** and requests for materials should be addressed to Jesús Gómez-Gardeñes or Alex Arenas.

**Peer review information** *Communications Physics* thanks the anonymous reviewers for their contribution to the peer review of this work.

**Reprints and permission information** is available at <http://www.nature.com/reprints>

**Publisher's note** Springer Nature remains neutral with regard to jurisdictional claims in published maps and institutional affiliations.



**Open Access** This article is licensed under a Creative Commons Attribution 4.0 International License, which permits use, sharing, adaptation, distribution and reproduction in any medium or format, as long as you give appropriate credit to the original author(s) and the source, provide a link to the Creative Commons license, and indicate if changes were made. The images or other third party material in this article are included in the article's Creative Commons license, unless indicated otherwise in a credit line to the material. If material is not included in the article's Creative Commons license and your intended use is not permitted by statutory regulation or exceeds the permitted use, you will need to obtain permission directly from the copyright holder. To view a copy of this license, visit <http://creativecommons.org/licenses/by/4.0/>.

© The Author(s) 2022